

1  
2  
3  
4  
5  
6  
7  
8  
9  
10  
11  
12  
13  
14  
15  
16  
17  
18  
19  
20  
21

# Supplementary Information for

## **Disproportionate increase in freshwater methane emissions induced by experimental warming**

Yizhu Zhu<sup>1</sup>, Kevin J Purdy<sup>2</sup>, Özge Eyice<sup>1</sup>, Lidong Shen<sup>1,3</sup>, Sarah F Harpenslager<sup>1,4</sup>, Gabriel Yvon-Durocher<sup>5</sup>, Alex J. Dumbrell<sup>6</sup>, Mark Trimmer<sup>1\*</sup>

### **Affiliations:**

<sup>1</sup>School of Biological and Chemical Sciences, Queen Mary University of London, London, E1 4NS, UK.

<sup>2</sup>School of Life Sciences, University of Warwick, Coventry, CV4 7AL, UK.

<sup>3</sup>Institute of Ecology, School of Applied Meteorology, Nanjing University of Information Science and Technology, Nanjing 210044, China.

<sup>4</sup>Leibniz Institute of Freshwater Ecology and Inland Fisheries (IGB), Department of Ecosystem Research, 12587, Berlin, Germany.

<sup>5</sup>Environment and Sustainability Institute, University of Exeter, Penryn Campus, Penryn, Cornwall, TR10 9FE, UK.

<sup>6</sup>School of Life Sciences, University of Essex, Colchester, Essex, U.K. CO4 3SQ.

### **This Supplementary Information includes:**

Supplementary Discussion

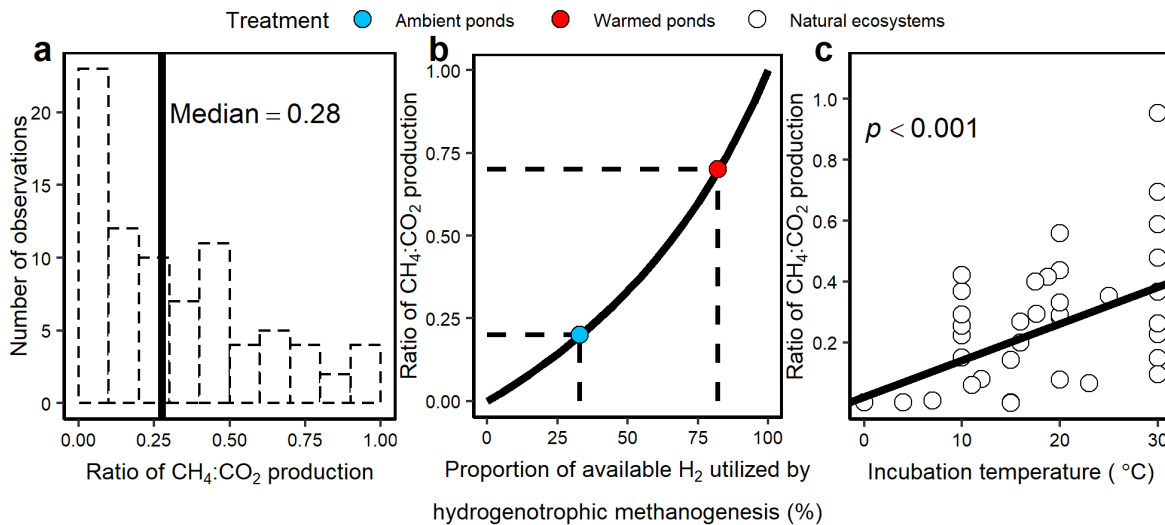
Supplementary Fig. 1 to 6

Supplementary Tables 1 to 10

## 22 Supplementary Discussion

### 23 The production of both CH<sub>4</sub> and CO<sub>2</sub> by a combination of acetoclastic and hydrogenotrophic 24 methanogenesis in relation to Ralf Conrad's 1999 publication (Ref. 24 in main text)

25 Determining the absolute ratio of CH<sub>4</sub>:CO<sub>2</sub> from any substrate via methanogenesis is challenging. Conrad  
26 (Ref. 24 in main text) calculated the idealised outcome of glucose degradation in a strictly methanogenic  
27 system, which does return a 1:1 ratio of CH<sub>4</sub> and CO<sub>2</sub>, via 33% hydrogenotrophic and 67% acetoclastic  
28 methanogenesis. However, he then shows that this idealised ratio is rarely true in nature where a strictly  
29 methanogenic system simply does not exist (and *see* Ref. 28 and 34 cited in the main text). Indeed here,  
30 we have compiled CH<sub>4</sub> and CO<sub>2</sub> production data from 13 studies including wetlands<sup>1-11</sup>, permafrost  
31 thaw<sup>12</sup> and lakes<sup>13</sup> which demonstrate that the vast majority of CH<sub>4</sub>:CO<sub>2</sub> production ratios are less than 0.5  
32 with a median of 0.28 only (*see* panel **a** in the figure below). Thus, in reality, Conrad's idealised ratio  
33 appears to be rare in natural systems and the same is true in our experimental ponds where the CH<sub>4</sub>:CO<sub>2</sub>  
34 ratios are less than 1:1 in both the ambient and warmed ponds (0.2:1 vs. 0.7:1).

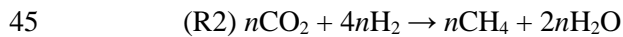


35  
36 Given that the carbon quality is similar between the warmed and ambient ponds (*see* Fig. 2b in main text),  
37 why has the CH<sub>4</sub>:CO<sub>2</sub> ratio increased after eleven years' warming? Here Conrad's model can be used to  
38 consider what a change in the CH<sub>4</sub> to CO<sub>2</sub> ratio might mean. Conrad's concept (ref. 24) through  
39 fermentation assumes that:

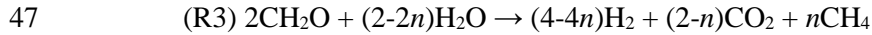


41 In most freshwater ecosystems where inorganic electron acceptors other than CO<sub>2</sub> are not available,  
42 hydrogenotrophic methanogenesis competes against homoacetogenesis for electrons from H<sub>2</sub>. We can

43 assume that the proportion of available H<sub>2</sub> utilized by hydrogenotrophic methanogenesis is  $n$  ( $0 < n < 1$ ) and  
44 by multiplying everything in hydrogenotrophic methanogenesis with  $n$  as a factor we get:



46 The sum of reaction (R1) and (R2) is:



48 The ratio of CH<sub>4</sub> to CO<sub>2</sub> produced is therefore  $n/(2-n)$ . The 1:1 ratio of CH<sub>4</sub> to CO<sub>2</sub> production occurs  
49 only when 100% of H<sub>2</sub> produced via fermentation (R1) is used up to reduce CO<sub>2</sub> to CH<sub>4</sub> (i.e.,  $n=1$ ), the  
50 CH<sub>4</sub>:CO<sub>2</sub> production ratio is however  $< 1:1$  when homoacetogenesis outcompetes hydrogenotrophic  
51 methanogenesis for H<sub>2</sub> and electrons flow to acetate rather than CH<sub>4</sub> ( $n < 1$ ). More importantly, (R3)  
52 predicts that the ratio of CH<sub>4</sub> to CO<sub>2</sub> increases exponentially as a function of the proportion of available  
53 H<sub>2</sub> being utilized by hydrogenotrophic methanogenesis ( $n$ ) (*see panel b* in the figure above). As H<sub>2</sub>  
54 becomes more available at higher temperatures<sup>13</sup>, should an increasing CH<sub>4</sub>:CO<sub>2</sub> ratio with temperature be  
55 expected? Indeed, this hypothesis is validated by a positive correlation between incubation temperatures  
56 and CH<sub>4</sub>:CO<sub>2</sub> ratios produced in anoxic wetland soils<sup>1,6,8,14</sup> (*see panel c* in the figure above). Therefore, an  
57 idealized 1:1 ratio is rare in reality but the CH<sub>4</sub>:CO<sub>2</sub> ratio increases towards the idealized 1:1 ratio  
58 predicted by Conrad at higher temperatures.

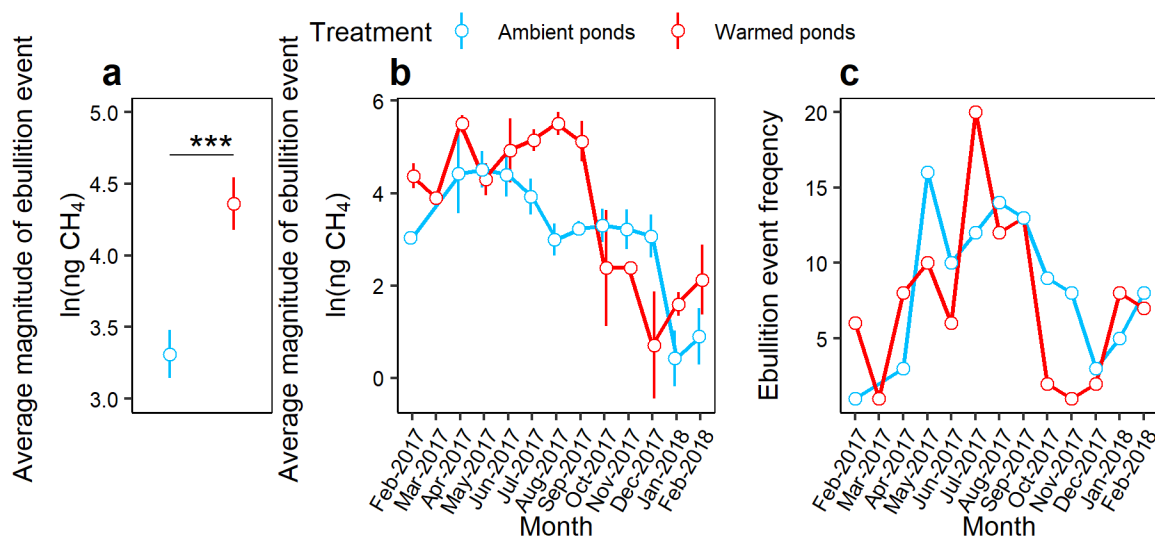
59 Furthermore, now we can rationalize the disproportionate increase in CH<sub>4</sub>:CO<sub>2</sub> production ratio seen in  
60 our long-term warmed ponds using the proportion of available H<sub>2</sub> being utilized by hydrogenotrophic  
61 methanogenesis. At lower temperatures, electrons flow to acetate and as a result methane production is  
62 dominated by acetoclasty<sup>15</sup> and only a minor proportion of available H<sub>2</sub> is utilized by hydrogenotrophic  
63 methanogenesis (30 %, the blue dot in panel **b**, *see figure above*). In contrast, as H<sub>2</sub> concentrations  
64 increase with temperature, which thermodynamically favours hydrogenotrophic methanogenesis, a larger  
65 proportion of electrons and carbon flow to CH<sub>4</sub> (80 %, the red dot in panel **b**, *see figure above*), ultimately  
66 increasing the CH<sub>4</sub> to CO<sub>2</sub> ratio closer towards the idealised ratio predicted by Conrad. In Figure 3d of the  
67 main text, we show clearly that hydrogenotrophic methanogenesis is favoured by warming and so  
68 conclude that, from whatever source, more of the available hydrogen is being directed more efficiently  
69 into methane in the warmed compared to the ambient ponds and that such disproportionate increase in  
70 CH<sub>4</sub>:CO<sub>2</sub> ratio will probably occur in natural freshwaters as the Earth warms.

71

72 **Supplementary Figures**

73 **Supplementary Fig. 1 | Magnitude and frequency of methane emission through ebullition events**  
 74 **( $n=198$ , 1.2% identified of the 16504 total chamber measurements using our two criteria and**  
 75 **exclusion of 7 other non-steady flux events – see Methods).**

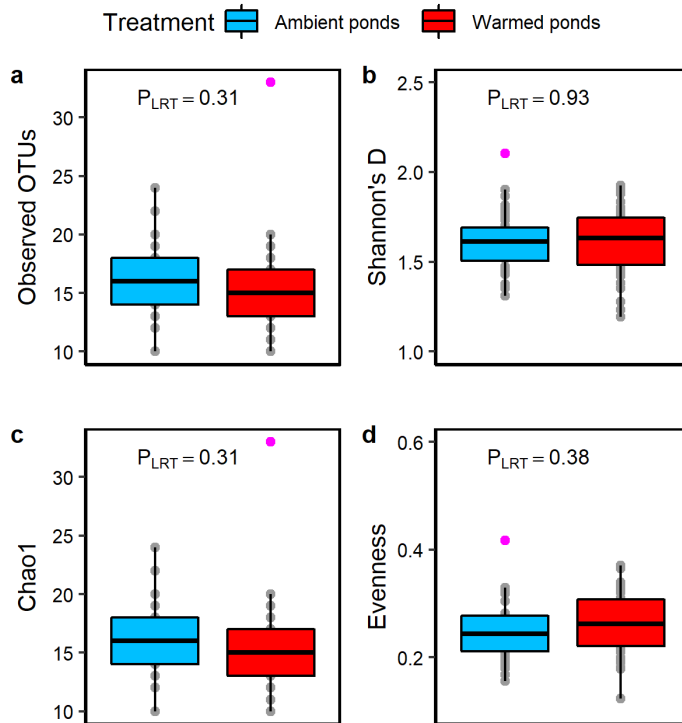
76 Ebullition in our ponds exports methane from the sediments to the atmosphere directly and therefore: **1**,  
 77 should increase with enhanced methanogenesis under warming; and **2**, follow a similar seasonal pattern to  
 78 diffusion. Indeed, in line with our enhanced methanogenesis under warming, the average magnitude of  
 79 ebullition events **a**, was 3-fold greater in the warmed ponds (80 ng CH<sub>4</sub> per event versus 27 ng CH<sub>4</sub> per  
 80 event in the ambient ponds, *t*-statistic, \*\*\*:  $p < 0.001$ ). In addition, the magnitude of ebullition events **b**,  
 81 and their frequency **c**, peaked in summer, demonstrating a similar seasonal pattern to diffusional methane  
 82 emissions (Extended Data Fig. 2). Ebullition events in our ponds have therefore been captured. However,  
 83 ebullition contributed only 0.2% of total methane emissions in both warmed and ambient ponds. The  
 84 magnitude of ebullition events was calculated using the maximum methane concentration in a chamber  
 85 measurement - see equation (1) in Methods. Error bars are standard errors of the magnitude of an  
 86 ebullition event.



87

88

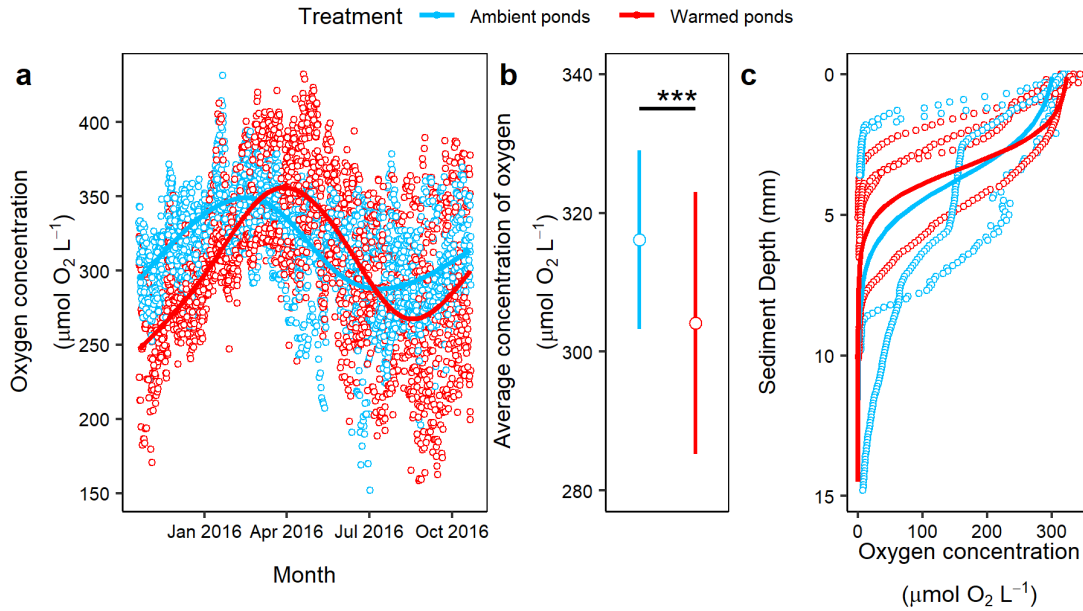
89 **Supplementary Fig. 2 | Methanogen alpha diversity ( $n=79$ , monthly samples from April to August**  
 90 **in 2016 from 8 ambient and 8 warmed ponds, see Methods). a**, Observed OTUs, **b**, Shannon's  
 91 diversity, **c**, Chao 1 diversity and **d**, evenness are all practically the same between the warmed (red) and  
 92 ambient (blue) ponds. Statistical significance ( $P_{LRT}$ ) was determined by a likelihood ratio test. Box lower  
 93 and upper bounds are 25th and 75th percentiles, respectively, the line is the median. Whiskers indicate  
 94 largest/smallest value no further than 1.5 times the interquartile range. The data points (in magenta)  
 95 beyond the end of whiskers are outliers.



96

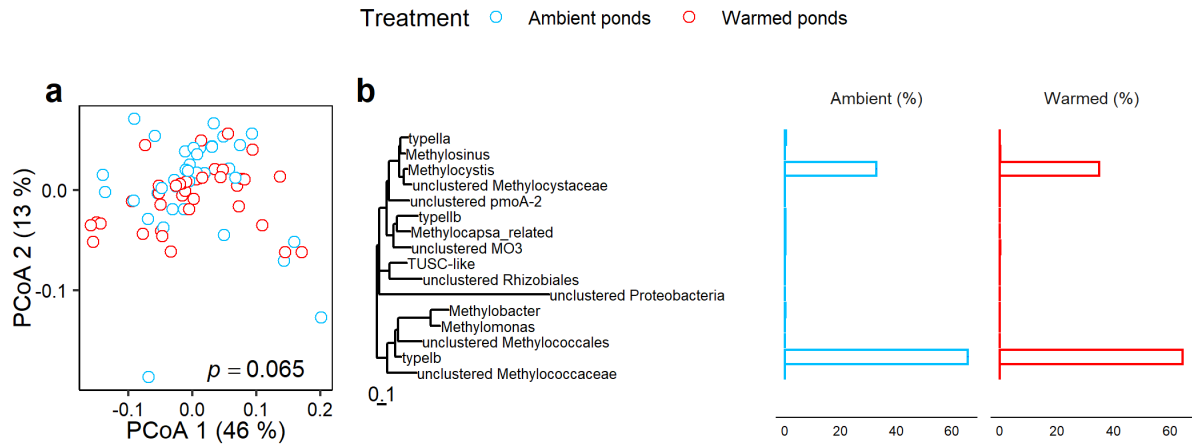
97

98 **Supplementary Fig. 3 | Water column and sediment oxygen concentrations in the experimental**  
 99 **ponds. a**, Seasonality of the *in situ* dissolved oxygen concentrations in the overlying water of the warmed  
 100 (red) and ambient (blue) ponds from October, 2015 to October, 2016 ( $n=5120$ , data collected at 10-  
 101 minute intervals using oxygen sensor in 7 ambient and 7 warmed). **b**, Mean *in situ* dissolved oxygen  
 102 concentration was lower in the warmed ponds compared to their ambient controls ( $n=5120$ ,  $t$ -statistic,  
 103  $p<0.001$ ). **c**, Oxygen penetration profiles measured in intact sediment cores at 15 °C ( $n=6$ , from 3 warmed  
 104 and 3 ambient in April, 2016). Oxygen concentrations showed a steeper decline and penetrated to a  
 105 shallower depth in the warmed pond sediment (4.86 mm) compared to 6.67 mm to the ambient pond  
 106 sediments.



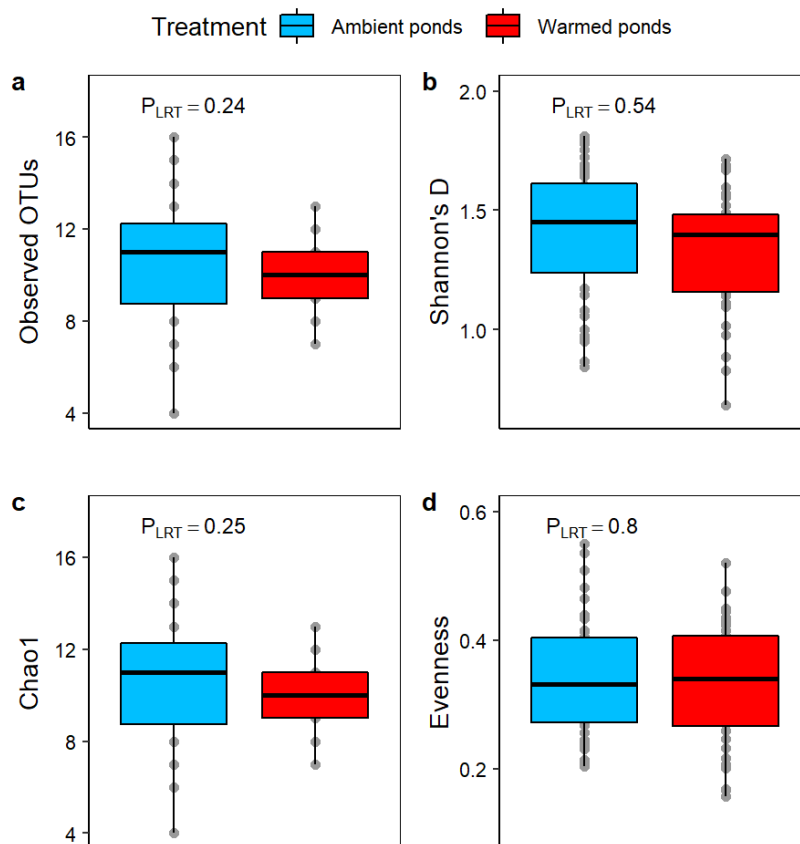
107  
 108

109 **Supplementary Fig. 4 | Effect of long-term warming on the methanotroph community composition**  
 110 **( $n=80$ , monthly samples from March to July in 2017 from 8 ambient and 8 warmed ponds, see**  
 111 **Methods). a**, No overall change in the methanotroph community with long-term warming demonstrated  
 112 by principal coordinate analysis (PCoA) using Bray-Curtis analysis and a Hellinger standardized dataset  
 113 (at genus level) and **b**, differential abundance analysis at genus level detected no significant changes in  
 114 any methanotroph genus.



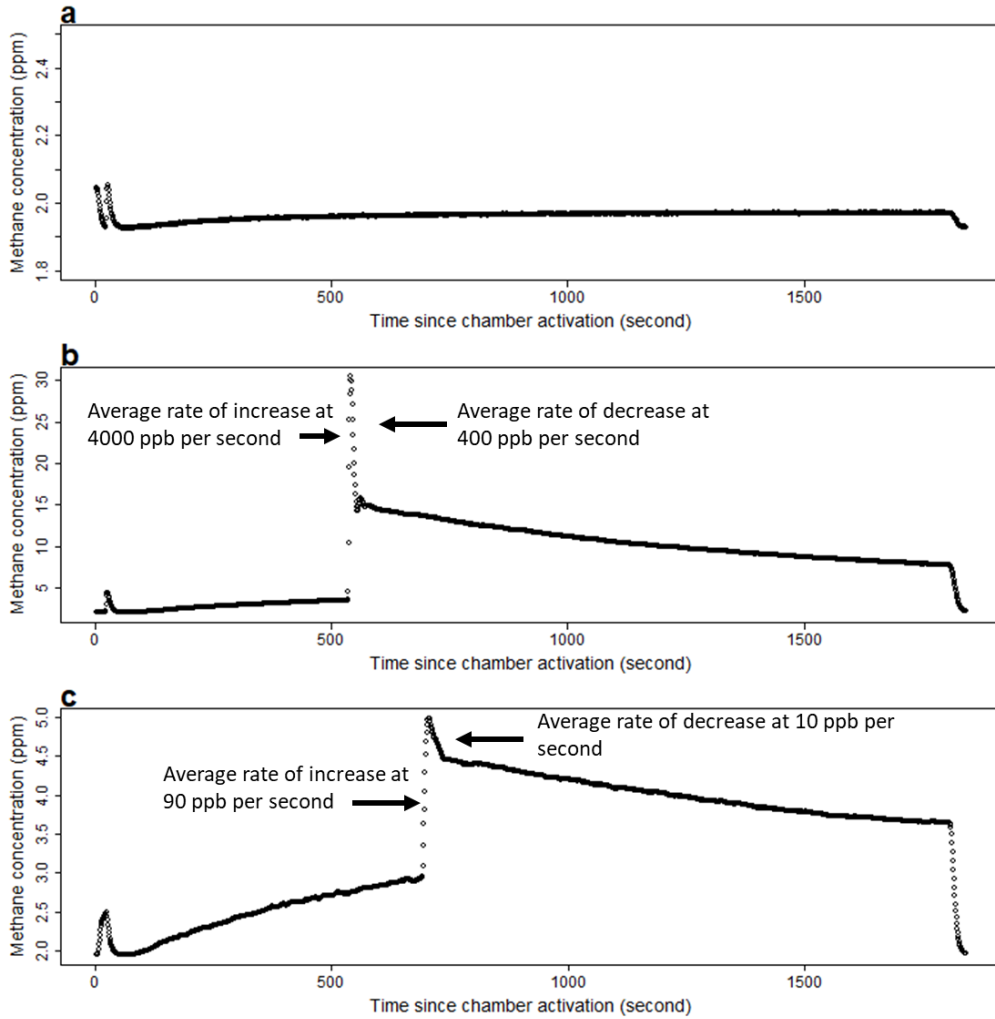
115  
116

117 **Supplementary Fig. 5 | Methanotroph alpha diversity ( $n=80$ , monthly samples from March to July**  
 118 **in 2017 from 8 ambient and 8 warmed ponds, see Methods). a, Observed OTUs, b, Shannon's**  
 119 **diversity, c, Chao 1 diversity and d, evenness are practically the same between the warmed (red) and**  
 120 **ambient (blue) ponds. Statistical significance ( $P_{LRT}$ ) was determined by a likelihood ratio test. Box lower**  
 121 **and upper bounds are 25th and 75th percentiles, respectively, the line is the median. Whiskers indicate**  
 122 **largest/smallest value no further than 1.5 times the interquartile range.**



123  
 124

125 **Supplementary Fig. 6 | Example of chamber measurements for a, steady-state flux b, strong**  
126 **ebullition and c, gentle ebullition.** Chambers with a steady state flux (a) had standing methane  
127 concentrations of ~2 ppm. When a strong ebullition event occurred methane rose very rapidly to 30 ppm  
128 at ~ 4,000 ppb/s, while, in gentler ebullition events (c), methane concentrations could increase at 90 ppb/s  
129 to ~5 ppm. In both cases methane concentrations subsequently decreased more gently than the rapid  
130 increase.



131

132

133

134

## Supplementary Tables

135 **Supplementary Table 1 | Original data sources for the analysis of methane emission capacities from**  
 136 **globally distributed sites.** Lat and Long represent latitude and longitude of each site. Avg. Temp =  
 137 average annual temperature in each site. *n* represents the number of daily rate measurements of methane  
 138 emissions for each site. The *p* values are less than 0.05 for each site, representing a good relationship  
 139 between methane emission and air-temperature.

Site ID	Site Name	Lat	Long	Avg. Temp (°C)	Type	<i>n</i>	<i>p</i> value	Ref.
AT-Neu	Neustift	47.12	11.31	10.0	Grassland	539	<0.05	
CA-SCB	Scotty Creek Bog	61.31	-121.3	11.8	Wetland	639	<0.05	16
FR-LGt	La Guette	47.32	2.28	13.4	Wetland	215	<0.05	
US-CRT	Curtice Walter-Berger cropland	41.63	-83.35	7.2	Cropland	246	<0.05	17
US-EML	Eight Mile Lake Permafrost thaw gradient, Healy Alaska.	63.88	-149.25	3.6	Open shrubs	1015	<0.05	18
US-LA1	Pointe-aux-Chenes Brackish Marsh	29.50	-90.45	22.9	Wetland	206	<0.05	19
US-LA2	Salvador WMA Freshwater Marsh	29.86	-90.29	24.0	Wetland	531	<0.05	20
US-Los	Lost Creek	46.08	-89.98	6.9	Wetland	1499	<0.05	21
US-Myb	Mayberry Wetland	38.05	-121.77	17.1	Wetland	2687	<0.05	22
US-ORv	Olentangy River Wetland Research Park	40.02	-83.02	13.3	Wetland	1132	<0.05	23
US-OWC	Old Woman Creek	41.38	-82.51	20.3	Wetland	104	<0.05	24
US-PFa	Park Falls/WLEF	45.95	-90.27	6.9	Forest	975	<0.05	25
US-Sne	Sherman Island Restored Wetland	38.04	-121.76	16.1	Wetland	575	<0.05	26
US-StJ	St Jones Reserve	39.09	-75.44	18.0	Wetland	250	<0.05	27
US-Tw1	Twitchell West Pond Wetland	38.11	-121.65	18.6	Wetland	2039	<0.05	28
US-Tw4	Twitchell East End Wetland	38.10	-121.64	17.5	Wetland	1668	<0.05	29
US-Twt	Twitchell Island	38.11	-121.65	18.2	Cropland	351	<0.05	30
US-Uaf	University of Alaska, Fairbanks	64.87	-147.86	12.0	Forest	236	<0.05	31
US-WPT	Winous Point North Marsh	41.46	-82.99	11.3	Wetland	793	<0.05	32

140 **Supplementary Table 2 | Annual methane budget, pond water characteristics and pond sediment**  
 141 **characteristics.**

		<b>Ambient</b>	<b>Warmed</b>	<b>Ratio (W/A)</b>
Production	Methane production capacity at 15 °C <sup>1</sup> (MG <sub>T15</sub> , μmol CH <sub>4</sub> m <sup>-2</sup> d <sup>-1</sup> )	2795 (1092)	7086 (2767)	2.5
	Effect of 4 °C warming predicted using the apparent activation energy $\overline{E_{MP}}$ (Effect <sub>warming</sub> ) <sup>2</sup>	1	1.5	1.5
	<b>Methane production capacity (totMG)<sup>3</sup></b>	2795	10274	<b>3.7</b>
	<i>mcrA</i> abundance (log <sub>10</sub> (copy g <sup>-1</sup> (wet sediments)))	6.59 (0.045)	6.77 (0.034)	1.5
	Methanogen cell-specific activity (fmol CH <sub>4</sub> <i>mcrA</i> <sup>-1</sup> h <sup>-1</sup> )	0.35	0.59	1.7
Emission and proportion of CH <sub>4</sub> oxidized <i>in situ</i>	Annual methane emission (ME, μmol CH <sub>4</sub> m <sup>-2</sup> d <sup>-1</sup> )	233 (22)	562 (63)	2.4
	<b>Amount of methane oxidized <i>in situ</i><sup>4</sup></b> <b>(<i>in situ</i> totMO, μmol CH<sub>4</sub> m<sup>-2</sup> d<sup>-1</sup>)</b>	2563	9713	<b>3.8</b>
	Proportion of methane oxidized <i>in situ</i> <sup>5</sup> (MO%, %)	92	95	1.03
	<b>Required proportion of CH<sub>4</sub> oxidized (%<sub>pred</sub>)<sup>6</sup></b>		<b>98</b>	
Oxidation	Kinetic effect of <i>in situ</i> methane concentrations (Effect <sub>kinetic</sub> ) <sup>7</sup>	1	1.9	1.9
	Effect of 4 °C warming predicted using apparent activation energy $\overline{E_{MO}}$ (Effect <sub>warming</sub> ) <sup>2</sup>	1	1.4	1.4
	Effect of sampling depth (Effect <sub>sampling</sub> ) <sup>8</sup>	1	1.4	1.4
	<b>Methane oxidation capacity (<i>ex situ</i> totMO)<sup>9</sup></b>			<b>3.6</b>
	<i>pmoA</i> abundance (log <sub>10</sub> (copy g <sup>-1</sup> (wet sediments)))	3.99 (0.047)	4.38 (0.038)	2.45
	Predicted fold increase in <i>pmoA</i> abundance to offset warming-induced methane production (Ab <sub>pred</sub> ) <sup>10</sup>			2.67
	Methanotroph cell-specific activity (pmol CH <sub>4</sub> <i>pmoA</i> <sup>-1</sup> h <sup>-1</sup> )	25.0	10.2	0.4
Water characteristic	Dissolved CH <sub>4</sub> concentration (μmol L <sup>-1</sup> )	0.51 (0.15)	1.07 (0.21)	2.1
Sediment characteristic	Sediment % carbon	0.83 (0.089)	1.23 (0.13)	1.48
	Sediment % nitrogen	0.084 (0.0061)	0.11 (0.0010)	1.31
	Sediment C:N	9.37 (0.41)	10.40 (0.31)	1.11

142 Numbers given in the brackets are standard errors.

143 1. Methane production capacity at 15 °C was calculated by taking the exponential of the ln-transformed

144 methane production rate in equation (4) ( $\overline{\ln F(T_C)}$ ) and converting from nmol g<sup>-1</sup> h<sup>-1</sup> to μmol m<sup>-2</sup> d<sup>-1</sup>

145 (sediment density 1,068 Kg m<sup>-3</sup> and depth 0.08 m) (MG<sub>T15</sub> =  $\overline{\ln F(T_C)} \times 10^6 \times 24 \times 1.068 \times 10^6 \times 0.08$ )

146 2. Effect of 4 °C warming on methane production and oxidation was calculated from the apparent  
147 activation energies:  $\overline{E}_{MP}$  and  $\overline{E}_{MO}$  for methane production and oxidation, respectively (*see* equations (2)  
148 and (4)). Apparent activation energies for methane production and oxidation in the warmed ponds are 0.7  
149 eV and 0.57 eV, respectively, predicting a 1.5- and 1.4-fold increase in the methane production and  
150 oxidation, respectively.

151 3. In total, methane production capacity in the warmed ponds increased by 3.7-fold  
152 ( $\text{totMG} = \text{MG}_{T15} \times \text{Effect}_{\text{warming}}$ ).

153 4. Total methane oxidized *in situ* is the difference between methane production capacity and annual  
154 methane emission (i.e., *in situ* totMO = totMG - ME)

155 5. Proportion of oxidized methane is the percentage of methane emission to methane production capacity  
156 at annual average temperatures (i.e.,  $\text{MO}\% = (\text{totMG} - \text{ME}) / \text{totMG} \times 100\%$ ).

157 6. Proportion of methane oxidation required in the warmed ponds to prevent methane emissions from  
158 increasing (i.e.,  $(\text{totMG}_{\text{warmed}} - \text{ME}_{\text{ambient}}) / \text{totMG}_{\text{warmed}} \times 100\%$ ).

159 7. Methane oxidation capacities at *in situ* methane concentrations were calculated using Michaelis-  
160 Menten model based on the methane concentrations in the pond water (*see* equation (7)).

161 8. Oxygen penetrated 4.86 and 6.67 mm into the warmed and ambient pond sediments, respectively  
162 (Supplementary Fig. 3). These depths were used as proxy for the active methanotrophy layer. Therefore,  
163 the effect of sampling the same depths in the warmed and ambient ponds for methane oxidation capacity  
164 measurements is  $\text{Effect}_{\text{sampling}} = \frac{20 \text{ mm}}{4.86 \text{ mm}} / \frac{20 \text{ mm}}{6.67 \text{ mm}}$ .

165 9. In total, warming increased the measured methane oxidation capacity in the warmed ponds by 3.6-fold  
166 ( $\text{Effect}_{\text{kinetic}} \times \text{Effect}_{\text{warming}} \times \text{Effect}_{\text{sampling}}$ ), accounting for the discrepancy between predicted and measured  
167 methane emissions *in situ* (*ex situ* totMG = *in situ* totMO).

168 10. Warming has increased the methane oxidation capacity by 3.6-fold but not the 3.9-fold required to  
169 offset the greater warming-induced methane production (i.e.,  $(\text{totMG}_{\text{warmed}} - \text{ME}_{\text{ambient}}) / (\text{totMG}_{\text{ambient}} -$   
170  $\text{ME}_{\text{ambient}})$ ). Predicted methanotroph abundance ( $\text{Ab}_{\text{pred}}$ ) to offset the greater warming-induced methane  
171 production is therefore the abundance of methanotroph required to achieve the predicted 3.9-fold methane  
172 oxidation capacity in warmed pond sediment if the efficiency per methanotroph stays the same (i.e., 10.2  
173 pmol CH<sub>4</sub> pmoA<sup>-1</sup>h<sup>-1</sup>).

174 *In situ* methane oxidation is limited by the diffusion of methane and oxygen. We acknowledge that by  
175 mixing the sediments and <sup>13</sup>C-CH<sub>4</sub> in our laboratory slurry measurements we would have optimized the

176 methane oxidation capacity in the sediments from both the warmed and ambient ponds. Therefore, we  
177 represent here, for the *ex situ* methane oxidation capacity, only the ratio between the warmed and ambient  
178 pond sediments (ratio W/A) to show that the kinetic effect and temperature effect increased the methane  
179 oxidation capacity by 1.9- and 1.4-fold in the warmed ponds relative to their ambient counterparts,  
180 respectively. In addition, if the depth of oxygen penetration serves as a proxy for active methanotrophy  
181 layer, altogether, the *ex situ* methane oxidation capacity in the warmed ponds would be 3.6-fold higher  
182 than in the ambient controls, close to the increase in methane production in the warmed ponds i.e. 3.7-  
183 fold, as well as the predicted amount of methane oxidized *in situ* i.e. 3.8-fold.

184

185 **Supplementary Table 3 | Linear mixed-effect model results for the  $\beta$ -diversity analysis of *mcrA***  
 186 **library ( $n=79$ , monthly samples from April to August in 2016 from 8 ambient and 8 warmed ponds,**  
 187 ***see Methods*) and *pmoA* library ( $n=80$ , monthly samples from March to July in 2017 from 8 ambient**  
 188 **and 8 warmed ponds, *see Methods*).**

189 The  $\beta$ -diversity was estimated using the scores along the first two principle coordinate axis (PCoA1 and  
 190 PCoA2) of the Bray-Curtis distance measures. These were then fitted into a mixed-effects model with  
 191 pond and sampling month treated as random effects. The statistical significance of the treatment (i.e.,  
 192 ambient or warmed ponds) was determined from the *F*-test using Satterthwaite's method for denominator  
 193 degrees-of-freedom and *F*-statistic. The results were similar to a PERMANOVA analysis.

Treatment	PCoA1			PCoA2		
	% Variation <sup>1</sup>	F-value	P-value	% Variation <sup>1</sup>	F-value	P-value
<i>mcrA</i>	34.04	6.13	<b>&lt;0.05</b>	22.93	3.54	<b>&lt;0.10</b>
<i>pmoA</i>	46.20	0.037	0.85	13.89	0.46	0.51

194 <sup>1</sup>. The amount of variation captured in the axis is defined as the proportion of eigenvalue of that axis  
 195 to the sum of all eigenvalues.

196  
 197

198 **Supplementary Table 4 | Taxonomy assignment to the *mcrA* OTUs at 85 % identity ( $n=79$ , monthly**  
 199 **samples from April to August in 2016 from 8 ambient and 8 warmed ponds, see Methods). Numbers**  
 200 **in parentheses are standard errors.**

Family	Genus	Sequence reads	
		Ambient	Warmed
<b><u>Hydrogenotrophic methanogens</u></b>			
unclustered <i>Methanomicrobiales</i>	unclustered <i>Methanomicrobiales</i>	227,766 (558)	225,753 (1,304)
<i>Methanospirillaceae</i>	<i>Methanospirillum</i>	256,777 (583)	184,696 (1,169)
<i>Methanobacteriaceae</i>	<i>Methanobacterium</i>	69,265 (210)	107,752 (398)
<i>Methanomicrobiaceae</i>	<i>Methanoplanus</i>	316 (3)	320 (7)
<i>Methanomicrobiaceae</i>	<i>Methanomicrobium</i>	174 (2)	223 (5)
<i>Methanocellaceae</i>	<i>Methanocella</i>	149 (3)	83 (2)
<i>Methanothermaceae</i>	<i>Methanothermus</i>	141 (1)	161 (2)
<i>Methanocaldococcaceae</i>	<i>Methanocaldococcus</i>	69 (1)	13 (0.3)
<i>Methanobacteriaceae</i>	<i>Methanothermobacter</i>	0 (0)	31 (1)
<i>Methanomicrobiaceae</i>	<i>Methanoculleus</i>	0 (0)	73 (2)
<b><u>Acetoclastic methanogens</u></b>			
<i>Methanosaetaceae</i>	<i>Methanosaeta</i>	257,132 (606)	287,992 (1,345)
<i>Methanosarcinaceae</i>	unclustered <i>Methanosarcinaceae</i>	7,285 (42)	5,071 (44)
<b><u>Methylotrophic methanogens</u></b>			
unclustered <i>Thermoplasmata</i>	unclustered <i>Thermoplasmata</i>	648 (7)	271 (7)
<i>Methanosarcinaceae</i>	<i>Methanohalophilus</i>	394 (4)	1,012 (8)
<i>Methanoplasmatales</i>	unclustered <i>Methanoplasmatales</i>	46 (1)	28 (1)
<i>Methanosarcinaceae</i>	<i>Methanosalsum</i>	0 (0)	25 (1)
<i>Methanosarcinaceae</i>	<i>Methanomethylovorans</i>	0 (0)	320 (8)

201

202 **Supplementary Table 5 | Taxonomy assignment to the *pmoA* OTUs at 90 % identity (*n*=80, monthly**  
 203 **samples from March to July in 2017 from 8 ambient and 8 warmed ponds, see Methods).**  
 204 Highlighted warmed pond data were at a lower relative abundance in those ponds compared to the  
 205 ambient ponds. Numbers in parentheses are standard errors.

Family	Genus	Sequence reads	
		Ambient	Warmed
<i>Methylococcaceae</i>	Type Ib	713,570 (1,689)	597,859 (1,081)
<i>Methylocystaceae</i>	<i>Methylocystis</i>	357,045 (1,166)	324,967 (855)
<i>Methylocystaceae</i>	Type IIa	4,784 (59)	100 (2)
MO3	unclustered MO3	2,532 (53)	1,681 (26)
<i>Beijerinckiaceae</i>	<i>Methylocapsa</i> -related	2,399 (37)	5 (0.1)
<i>Environmental samples</i>	Type IIb	2,012 (26)	79 (1)
<i>Methylococcaceae</i>	TUSC-like	1,062 (12)	14 (0.4)
<i>Methylococcaceae</i>	<i>Methylobacter</i>	1,372 (13)	158 (3)
<i>Methylocystaceae</i>	<i>Methylosinus</i>	535 (7)	1,848 (18)
unclustered <i>Proteobacteria</i>	unclustered <i>Proteobacteria</i>	362 (5)	0 (0)
pmoA-2	unclustered pmoA-2	235 (4)	410 (5)
<i>Methylocystaceae</i>	unclustered <i>Methylocystaceae</i>	166 (2)	88 (2)
unclustered <i>Rhizobiales</i>	unclustered <i>Rhizobiales</i>	149 (2)	12 (0.3)
<i>Methylococcaceae</i>	<i>Methylomonas</i>	13 (0.3)	0 (0)
unclustered <i>Methylococcales</i>	unclustered <i>Methylococcales</i>	0 (0)	181 (4)
<i>Methylococcaceae</i>	unclustered <i>Methylococcaceae</i>	0 (0)	28 (1)

206  
207

208 **Supplementary Table 6 | Multi-model selection for fitting generalized additive mixed effects models**  
 209 **to the seasonal CH<sub>4</sub> emission data (*n*=3553 steady-state estimates, representing emissions from 7**  
 210 **ambient and 7 warmed ponds with each pond being notionally measured three times per day – see**  
 211 **Methods ).**

212 To assess the effect of long-term warming on the median rate of methane emissions, a range of  
 213 generalized additive mixed effects models (GAMMs) were fitted to the daily methane emission rate data  
 214 (ME) as a function of treatment (i.e., warmed or ambient pond) and day of the year since 1<sup>st</sup> January 2017  
 215 (DOY). Whether the seasonal pattern of methane emissions differed between the treatment was also  
 216 tested by comparing the smoother terms (DOY, by=Treatment) and s(DOY). Models were ranked using  
 217 the AIC. ΔAIC refers to differences in AIC relative to the smallest AIC value and AIC weight is the  
 218 probability of any model providing the best fit to the data e.g., 0.913 indicates that model (1) is the best fit  
 219 to the data.

	<b>Model</b>	<b>d.f.</b>	<b>AIC</b>	<b>ΔAIC</b>	<b>AIC Weight</b>
(1)	Ln(ME)~Treatment+s(DOY,by=Treatment)	8	12035.0	0.00	0.913
(2)	Ln(ME)~s(DOY,by=Treatment)	7	12039.7	4.71	0.087
(3)	Ln(ME)~Treatment+s(DOY)	6	12194.2	159.24	0.000
(4)	Ln(ME)~s(DOY)	5	12198.9	163.94	0.000

220 A GAMM which included treatment on the intercept and a treatment-specified smoother term for DOY  
 221 provided the best fit to the seasonal methane emission data, demonstrating an increase in median methane  
 222 emission from warmed ponds as well as a difference in seasonality.  
 223  
 224

225 **Supplementary Table 7 | Multi-model selection for fitting linear mixed-effect models to CH<sub>4</sub>**  
 226 **potential production data (nmol CH<sub>4</sub> g<sup>-1</sup>h<sup>-1</sup>) as a function of treatment (e.g. warmed or ambient**  
 227 **ponds), additional substrates and experimental incubation temperature (Ts) (n=662). Sediment**  
 228 **samples collected monthly and randomly from 3 to 5 of the 10 ambient and 3 to 5 of the 10 warmed**  
 229 **ponds with each incubated at 3 temperatures and with up to 2 substrates. The sample size for**  
 230 **control only, i.e., without additional substrates, of the total 662 samples, was 238. No replicate was**  
 231 **applied within each pond.**

232 Ts represents the standardized temperature  $\left(\frac{1}{kT_c} - \frac{1}{kT_{ij}}\right)$  in equation (4). A range of linear mixed-effect  
 233 models were fitted to the rate of methane production (ln(MG)) data. Note that only the fixed-effect parts  
 234 of the models are included in the table. As in Supplementary Table 6, models were ranked using the AIC  
 235 and an AIC weight of 0.76 indicates that model 1 is the best fit to the data.

	<b>Model</b>	<b>d.f.</b>	<b>AIC</b>	<b>ΔAIC</b>	<b>AIC Weight</b>
	Ln(MG)~Ts+Treatment+Substrate				
(1)	+Ts×Treatment+Ts×Substrate +Treatment×Substrate	13	1820.6	0.00	0.76
	Ln(MG)~Ts+Treatment+Substrate				
(2)	+Ts×Treatment+Ts×Substrate+ Treatment×Substrate+Ts×Treatment×Substrate	15	1823.4	2.78	0.19
	Ln(MG)~Ts+Treatment+Substrate				
(3)	+Ts×Substrate+Treatment×Substrate	12	1826.3	5.71	0.04
	Ln(MG)~Ts+Treatment+Substrate				
(4)	+Ts×Treatment+Ts×Substrate	11	1829.2	862	0.01
	Ln(MG)~Ts+Treatment+Substrate+Ts×Substrate				
(5)		10	1834.5	13.94	0.001

236 Note that in the incubations above 22°C the rate of CH<sub>4</sub> production plateaued and therefore we excluded  
 237 these data from the model.  
 238

239 **Supplementary Table 8 | Model selection procedure for fitting linear mixed-effect models to**  
 240 **sediment methane potential production data (MG) as a function of carbon turnover  $k$  ( $n=32$ ,**  
 241 **sediment samples collected from 4 ambient and 4 warmed ponds in April, May, June and August,**  
 242 **2017).**

243 The full model included additive terms and their interactions for two fixed effects – natural logarithm of  
 244 carbon turnover  $k$  ( $\ln k$ ) and treatment type (i.e., ambient or warmed ponds). The significance ( $p$ -values) of  
 245 the fixed-effect terms was determined using a likelihood ratio test on nested models. The  $p$ -value for  
 246 comparing “Treatment $\times\ln k$ ” was 0.40, and the term removed from the model. As removing  
 247 “Treatment $\times\ln k$ ” had no significant effect on model fit, model F1, that included a single slope but distinct  
 248 intercepts provided the best fit to the methane potential data (marked in bold), demonstrating that the  
 249 potential of sediments to produce methane increased equally in both the warmed and ambient pond  
 250 sediments as carbon quality also increased but warming has stepped-up the fraction of carbon respired to  
 251 methane.

Model	d.f.	AIC	LogLik	$p$ -value
F0) $\ln(\text{MG}) \sim \ln k \times \text{Treatment} + \ln k + \text{Treatment}$	6	94.2	-41.09	
<b>F1) <math>\ln(\text{MG}) \sim \ln k + \text{Treatment}</math></b>	<b>5</b>	<b>92.9</b>	<b>-41.44</b>	<b>0.40</b>
F2) $\ln(\text{MG}) \sim \ln k$	4	98.8	-45.4	<0.01
F3) $\ln(\text{MG}) \sim 1$	3	107.7	-50.9	<0.001

252  
 253

254 **Supplementary Table 9 | Model selection procedure for fitting mixed-effect models to methane**  
 255 **oxidation as a function of kinetic or temperature responses.**

256 **a, Fitting Michaelis-Menten models to CH<sub>4</sub> oxidation rate (MO) as a function of initial CH<sub>4</sub>**  
 257 **concentration (*n*=158, sediment samples collected from 8 ambient and 8 warmed ponds in July,**  
 258 **2017, and December, 2018, with a range of initial methane concentrations, see equation (7) in**  
 259 **Methods).** The full model included the initial methane concentrations ( $C_{CH_4}$ ) and the two Michaelis-  
 260 Menten parameters defining the kinetic response, i.e., the maximum methane oxidation rate ( $V_{max}$ ) and the  
 261 Michaelis constant ( $K_m$ ). The significance of treatment (i.e., warmed or ambient) on the parameters ( $V_{max}$   
 262 + Treatment) and ( $K_m$  + Treatment) was determined via Likelihood Ratio Test on nested models. As  
 263 removing the effect of treatment on  $K_m$  and  $V_{max}$  had no significant effect on model fit ( $p=0.98$  and  
 264  $p=0.45$ , respectively), the model with the same  $V_{max}$  and  $K_m$  terms for both warmed and ambient pond  
 265 sediments provided the best fit to the CH<sub>4</sub> oxidation data (model F2, marked on bold).

Model	d.f.	AIC	LogLik	<i>p</i> -value
F0) MO ~ ( $C_{CH_4}$ , $V_{max}$ +Treatment, $K_m$ +Treatment)	6	2106.21	-1047.10	
F1) MO ~ ( $C_{CH_4}$ , $V_{max}$ +Treatment, $K_m$ )	5	2104.21	-1047.10	0.98
<b>F2) MO ~ (<math>C_{CH_4}</math>, <math>V_{max}</math>, <math>K_m</math>)</b>	<b>4</b>	<b>2102.78</b>	<b>-1047.39</b>	<b>0.45</b>

266

267 **b, Model selection procedure for fitting linear mixed-effect models to the temperature sensitivity of**  
 268 **CH<sub>4</sub> oxidation rate (ln(MO)) (*n*=192, sediment samples collected from 8 warmed and 8 ambient**  
 269 **ponds in May, June and July, 2017, incubated under four different temperatures).** The full model  
 270 included additive terms and their interactions for two fixed effects – standardized temperature at 15 °C  
 271 (Ts, term  $\left(\frac{1}{kT_c} - \frac{1}{kT_{ij}}\right)$  in equation (4)) and treatment type (i.e., ambient or warmed ponds). The  
 272 significance of fixed-effect terms (*p*-values) were determined using a likelihood ratio test on nested  
 273 models. For example, the significance of the term “Treatment×Ts”, i.e., distinct slopes between warmed  
 274 and ambient pond sediments, was determined by comparing nested model F0 to its reduced model F1.  
 275 The *p*-value of this comparison was 0.24, the term “Treatment×Ts” was not significant and was thus  
 276 removed from the model. As removing “Treatment×Ts” or “Treatment” had no significant effect on  
 277 model fit, the model F2, that included a single slope and intercept, therefore provided the best fit to the  
 278 CH<sub>4</sub> oxidation rate data (marked in bold), demonstrating that the CH<sub>4</sub> oxidation capacity and its  
 279 temperature sensitivity were the same in both the warmed and ambient ponds.

Model	d.f.	AIC	LogLik	$\chi^2$	<i>p</i> -value
F0) ln(MO)~Ts+Treatment×Ts+Treatment	8	287.12	-135.56		
F1) ln(MO)~Ts+Treatment	7	286.48	-135.56	1.36	0.24
<b>F2) ln(MO)~Ts</b>	<b>6</b>	<b>287.81</b>	<b>-137.91</b>	<b>3.33</b>	<b>0.068</b>
F3) ln(MO)~1	5	329.75	-159.88	43.94	<0.001

280

281 **Supplementary Table 10 | Model selection procedure for fitting linear mixed-effect models to the**  
 282 **carbon conversion efficiency (CCE) data.**

283 **a, Carbon conversion efficiency as function of temperature** ( $n=191$ , sediment samples collected from  
 284 8 warmed and 8 ambient ponds in May, June and July, 2017, incubated under four different  
 285 temperatures). The full model included additive terms and their interactions for two fixed effects –  
 286 centered temperature at 15 °C ( $T_c$ , term  $T - T_c$  in equation (8)) and treatment types (i.e., ambient or  
 287 warmed ponds). The significance ( $p$ -values) of fixed-effect terms was determined using a likelihood ratio  
 288 test on nested models. As removing “Treatment $\times$  $T_c$ ” or “Treatment” had no significant effect on model  
 289 fit, the model, F2, that included one common slope and intercept provided the best fit to CCE data  
 290 (marked in bold).

Model	d.f.	AIC	LogLik	$\chi^2$	$p$ -value
F0) CCE~ $T_c$ +Treatment+ Treatment $\times$ $T_c$	8	1041.2	-512.61		
F1) CCE~ $T_c$ +Treatment	7	1039.5	-512.72	0.23	0.63
<b>F2) CCE~<math>T_c</math></b>	<b>6</b>	<b>1037.7</b>	<b>-512.84</b>	<b>0.23</b>	<b>0.63</b>
F3) CCE~1	5	1069.0	-529.51	33.34	<0.01

291  
 292 **b, Carbon conversion efficiency as function of methane concentration** ( $n=69$ , sediment samples  
 293 collected in July, 2017, from 8 ambient and 8 warmed ponds with a range of initial methane  
 294 concentrations): The full model included additive terms and their interactions for two fixed effects –  
 295 initial  $^{13}\text{C}$ - $\text{CH}_4$  concentration ( $C_{\text{CH}_4}$ , see equation (9)) and treatment type (i.e., ambient or warmed ponds).  
 296 The significance ( $p$ -value) of fixed-effect terms was determined using a likelihood ratio test on nested  
 297 models. As removing “ $C_{\text{CH}_4}\times$ Treatment” or “Treatment” had no significant effect on model fit, the model,  
 298 F2, that included one common slope and intercept provided the best fit to CCE data (marked in bold).

Model	d.f.	AIC	LogLik	$\chi^2$	$p$ -value
F0) CCE~ $C_{\text{CH}_4}$ +Treatment+ $C_{\text{CH}_4}\times$ Treatment	6	458.78	-223.39		
F1) CCE~ $C_{\text{CH}_4}$ +Treatment	5	456.86	-223.43	0.083	0.77
<b>F2) CCE~<math>C_{\text{CH}_4}</math></b>	<b>4</b>	<b>455.63</b>	<b>-223.82</b>	<b>0.77</b>	<b>0.38</b>
F3) CCE~1	3	463.93	-228.97	10.30	<0.01

## Supplementary References

- 301 1. Inglett, K. S., Inglett, P. W., Reddy, K. R. & Osborne, T. Z. Temperature sensitivity of greenhouse  
302 gas production in wetland soils of different vegetation. *Biogeochemistry* **108**, 77–90 (2012).
- 303 2. Hodgkins, S. B. *et al.* Changes in peat chemistry associated with permafrost thaw increase  
304 greenhouse gas production. *Proc. Natl. Acad. Sci. U. S. A.* **111**, 5819–5824 (2014).
- 305 3. Valentine, D. W., Holland, E. A. & Schimel, D. S. Ecosystem and physiological controls over  
306 methane production in northern wetlands. *J. Geophys. Res. Atmos.* **99**, 1563–1571 (1994).
- 307 4. Tfaily, M. M. *et al.* Journal of Geophysical Research: Biogeosciences. *J. Geophys. Res.*  
308 *Biogeosciences* **119**, 661–675 (2014).
- 309 5. Wright, E. L. *et al.* Contribution of subsurface peat to CO<sub>2</sub> and CH<sub>4</sub> fluxes in a neotropical  
310 peatland. *Glob. Chang. Biol.* **17**, 2867–2881 (2011).
- 311 6. Updegraff, K., Pastor, J., Bridgman, S. D. & Johnston, C. A. Environmental and substrate controls  
312 over carbon and nitrogen mineralization in northern wetlands. *Ecol. Appl.* **5**, 151–163 (1995).
- 313 7. Blodau, C. & Deppe, M. Humic acid addition lowers methane release in peats of the Mer Bleue  
314 bog, Canada. *Soil Biol. Biochem.* **52**, 96–98 (2012).
- 315 8. Kolton, M., Marks, A., Wilson, R. M., Chanton, J. P. & Kostka, J. E. Impact of warming on  
316 greenhouse gas production and microbial diversity in anoxic peat from a Sphagnum-dominated  
317 bog (Grand Rapids, Minnesota, United States). *Front. Microbiol.* **10**, 1–13 (2019).
- 318 9. Hodgkins, S. B. *et al.* Soil incubations reproduce field methane dynamics in a subarctic wetland.  
319 *Biogeochemistry* **126**, 241–249 (2015).
- 320 10. Keller, J. K. & Bridgman, S. D. Pathways of anaerobic carbon cycling across an ombrotrophic-  
321 minerotrophic peatland gradient. *Limnol. Oceanogr.* **52**, 96–107 (2007).
- 322 11. Bridgman, S. D., Johnston, C. A., Pastor, J. & Updegraff, K. Potential Feedbacks of Northern  
323 Wetlands on Climate Change. *Bioscience* **45**, 262–274 (1995).
- 324 12. McCalley, C. K. *et al.* Methane dynamics regulated by microbial community response to  
325 permafrost thaw. *Nature* **514**, 478–481 (2014).
- 326 13. Glissmann, K., Chin, K. J., Casper, P. & Conrad, R. Methanogenic pathway and archaeal  
327 community structure in the sediment of eutrophic Lake Dagow: Effect of temperature. *Microb.*  
328 *Ecol.* **48**, 389–399 (2004).
- 329 14. Keller, J. K., Weisenborn, P. B. & Megonigal, J. P. Humic acids as electron acceptors in wetland  
330 decomposition. *Soil Biol. Biochem.* **41**, 1518–1522 (2009).
- 331 15. Fey, A. & Conrad, R. Effect of Temperature on Carbon and Electron Flow and on the Archaeal  
332 Community in Methanogenic Rice Field Soil. *Appl. Environ. Microbiol.* **66**, 4790–4797 (2000).
- 333 16. Sonntag, O. & Quinton, W. L. AmeriFlux CA-SCB Scotty Creek Bog. (2016)  
334 doi:10.17190/AMF/1498754.
- 335 17. Chen & Jiquan. AmeriFlux US-CRT Curtice Walter-Berger cropland. (2016)  
336 doi:10.17190/AMF/1246156.
- 337 18. Schuur & Ted. AmeriFlux US-EML Eight Mile Lake Permafrost thaw gradient, Healy Alaska.  
338 (2018) doi:10.17190/AMF/1418678.
- 339 19. Krauss & Ken. AmeriFlux US-LA1 Pointe-aux-Chenes Brackish Marsh. (2016)  
340 doi:10.17190/AMF/1543386.
- 341 20. Krauss & Ken. AmeriFlux US-LA2 Salvador WMA Freshwater Marsh. (2016)  
342 doi:10.17190/AMF/1543387.
- 343 21. Desai & Ankur. AmeriFlux US-Los Lost Creek. (2016) doi:10.17190/AMF/1246071.
- 344 22. Baldocchi & Dennis. AmeriFlux US-Myb Mayberry Wetland. (2016)  
345 doi:10.17190/AMF/1246139.
- 346 23. Bohrer & Gil. AmeriFlux US-ORv Olentangy River Wetland Research Park. (2016)  
347 doi:10.17190/AMF/1246135.
- 348 24. Bohrer & Gil. AmeriFlux US-OWC Old Woman Creek. (2018) doi:10.17190/AMF/1418679.

- 349 25. Desai & Ankur. AmeriFlux US-PFa Park Falls/WLEF. (2016) doi:10.17190/AMF/1246090.  
350 26. Baldocchi & Dennis. AmeriFlux US-Sne Sherman Island Restored Wetland. (2018)  
351 doi:10.17190/AMF/1418684.  
352 27. Vargas & Rodrigo. AmeriFlux US-StJ St Jones Reserve. (2016) doi:10.17190/AMF/1480316.  
353 28. Baldocchi & Dennis. AmeriFlux US-Tw1 Twitchell Wetland West Pond. (2016)  
354 doi:10.17190/AMF/1246147.  
355 29. Baldocchi & Dennis. AmeriFlux US-Tw4 Twitchell East End Wetland. (2016)  
356 doi:10.17190/AMF/1246151.  
357 30. Baldocchi & Dennis. AmeriFlux US-Twt Twitchell Island. (2016) doi:10.17190/AMF/1246140.  
358 31. Iwata, H., Ueyama, M. & Harazono, Y. AmeriFlux US-Uaf University of Alaska, Fairbanks.  
359 (2016) doi:10.17190/AMF/1480322.  
360 32. Chen & Jiquan. AmeriFlux US-WPT Winous Point North Marsh. (2016)  
361 doi:10.17190/AMF/1246155.  
362